Location of Single Phase-Earth Faults in Distribution Networks based on Synchronous Transient Energy

Wang, Xuewen; Zhang, Hengxu; Shi, Fang; Wu, Qiuwei; Terzija, Vladimir; Xie, Wei; Fang, Chen

Published in:
IEEE Transactions on Smart Grid

Link to article, DOI:
10.1109/tsg.2019.2938667

Publication date:
2019

Document Version
Peer reviewed version

Location of Single Phase to Ground Faults in Distribution Networks based on Synchronous Transients

Xuewen Wang, *Student Member, IEEE*, Hengxu Zhang, *Member, IEEE*, Fang Shi, *Member, IEEE*, Qiuwei Wu, *Senior Member, IEEE*, Vladimir Terzija, *Fellow, IEEE,* Wei Xie *and* Chen Fang

***Abstract*—As a result of small fault current, high level of noise and a large penetration of distributed generators (DG), in the neutral non-effectively grounded medium-voltage (MV) distribution networks, it is quite difficult to locate the faulted line section for single phase to ground faults. In this paper, using a technique based on synchronized measurements in distribution networks, a fault location method based on the analysis of the energy of the transient zero-sequence current in the selected frequency band (SFB) is proposed. The equivalent impedance of the distribution network with lateral branches is studied with an equivalent network, and the phase-frequency characteristics of the equivalent impedance are analyzed. The SFB, within which the transient energy of the faulty line section is larger than that of the healthy line sections is determined. A combined fault-section location criterion is proposed and the implementation scheme is illustrated with the distribution level phasor measurement units. Numerical simulations of the IEEE 34 node system and the field experiments of a 10kV distribution network validate the feasibility and effectiveness of the proposed method.**

***Index Terms*-- Active distribution networks, fault location, neutral non-effectively grounded system, single phase to ground faults, transient zero-sequence current.**

I. Introduction

SINGLE phase to ground faults accounts for up to 80 percent of all the faults in distribution networks, and most of them are transient faults [1]. Unfortunately, it is difficult to locate these faults effectively and precisely, especially for the neutral non-effectively grounded medium-voltage (MV) distribution networks, which exist in China, Japan and some of the European countries. The advantage is that the power supply can last for a certain time after the ground faults occur as the fault current is limited. However, it will deteriorate the insulation of the equipment, cause short circuit faults [2]-[3] and threaten the safety of people or property. Therefore, efficient and accurate fault identification and location are important for electric utilities.

Most of the current techniques for single phase to ground fault location are specified for the detection and identification of the faulty feeders. These methods can be roughly categorized into three groups.

1) Using the steady-state signal. The amplitude and phase difference of the fundamental frequency zero-sequence current are widely used to detect the faulty feeder [6]-[10]. In [11], the 5th harmonic current was extracted for faulty line selection [11]. The zero-sequence admittance was calculated using zero-sequence voltage and current to identify the faulty line and faulty line section in [12]. These techniques only use the steady-state signals suitable for the steady-state ground fault, the information in the very early stage of the fault is neglected. As a result, these methods are not reliable for the transient fault or the resonant grounded system.

2) Using the transient signal. The transient signal is less affected by the neutral grounding mode, which makes it has a wider potential application. It is efficient to use the zero-sequence current travelling wave to detect the faulty feeder even when the fault resistance is high [13]-[14]. However, it is difficult to detect the faulty feeder when the voltage inception angle is near zero. The correlation analysis of the transient zero-sequence current waveform between the faulty and the healthy feeder was used for faulty feeder identification in [15]-[16]. The transient component of the zero-sequence current and voltage was used for calculating the transient energy of every feeder in [17], which may be affected by the noise and lead to mis-judgement when the fault resistance is high. In [18], using the wavelet packet transform method, the zero-sequence currents of feeders were decomposed into different frequency bands and a selected frequency band (SFB) was utilized for faulty feeder detection. Artificial intelligence (AI) methods were reported in [19], which largely depend on the reliability of the algorithms and the training database size. And it lacks of clear physical meaning and the high computational cost restrict the practical application of the AI techniques.

3) Active methods [20]-[26]. By injecting various frequency signals or controlling the compensation degree of the Peterson coil, the signals monitored in the faulty feeder are changed and the faulty feeder is detected. Different from the above methods, supplementary devices and extra operations are needed, which increase the potential risks and cost.

When the single phase to ground fault occurs in distribution networks, the fault signals are weak and heavily contaminated by noises, which makes it difficult to identify and locate the faults for industrial applications. The increasing penetration of the DGs and non-linear loads in the evolving active distribution networks further increases the difficulties. In [27], a wide-area high-frequency impedance comparison method is proposed based on the high-frequency impedance model for DGs without knowing exact parameters of the distribution

This work was supported by the National Key Research and Development Program of China (2017YFB0902800) and Science and Technology Project of State Grid Corporation of China (52094017003D).

Xuewen Wang, Hengxu Zhang and Fang Shi are with the Key Laboratory of Power System Intelligent Dispatch and Control of the Ministry of Education (Shandong University), Jinan, China (shifang@ sdu.edu.cn).

Qiuwei Wu is with Technical University of Denmark and is visiting professor at Shandong University.

Vladimir Terzija is with The University of Manchester and is visiting professor at Shandong University.

Wei Xie and Chen Fang are with State Grid Shanghai Municipal Electric Power Company, Shanghai, China.

system. In [28], the actual inverters' control strategies during faults of the photovoltaic (PV) power plants are considered, and the improved Bayesian compressive sensing algorithm is used to extract the fault characteristics and then locate the faulted node. The synchronous measurement can improve the effectiveness and feasibility of the above two methods. Besides, reliable power supply and high-speed restoration requirements have shown the need for an on-line and accurate fault location scheme. Therefore, the fault characteristics immune to noises and new centralized algorithms based on multi-measurements should be carefully studied. With the accessibility of the synchronized, low-latency and high-resolution measurement data from the distribution-level phasor measurement units (D-PMUs) [29]-[31], the synchronized phasor and sampling data can be acquired at the distribution control center for further applications.

This paper proposes a new scheme to locate the faulted line section in a short time after the single phase to ground fault, which is especially designed for the neutral non-effectively grounded MV distribution networks. By analyzing the equivalent zero-sequence circuit for the single phase to ground fault in distribution networks, the SFB is studied within which the transient zero-sequence current is far greater than the noises. Then, the frequency range of the SFB for a general distribution network with lateral branches is determined based on the phase-frequency characteristics of the equivalent network. The transient energy of the monitored voltage/current component within the SFB is calculated for each feeder section, which shows that the faulty feeder section has the largest transient energy. It is proven that the polarities of the zero-sequence currents are opposite between the faulty feeder section and the healthy ones. A new criterion combining the above two characteristics is proposed and the settings are established to determine the faulty line section. The procedures for practical application are illustrated with the increasing emergence of D-PMUs.

The rest of the paper is organized as follows. Section II describes the determination of the frequency range of the SFB by analyzing the phase-frequency characteristics of the equivalent network. In section III, a new criterion is proposed and the implementation of the new fault location scheme is illustrated. Section IV presents the testing results of the proposed scheme both with simulation data and the field data from fault experiments. Section V demonstrate the comparison results with three other methods. Conclusions are drawn in Section V.

II. PROBLEM FORMULATION

A. Phase-frequency characteristics of the distribution feeders

On the study of zero-sequence network of the neutral non-effectively grounded systems, there is no necessary to consider the effect of loads [25]. Furthermore, the primary sides of DG transformers are ungrounded [4], hence the zero-sequence circuit of the distribution networks with DGs are the same as that without DGs. Consequently, when a single phase to ground fault occurs at the end of the feeder, the zero-sequence distributed parameter equivalent circuit of the neutral non-effectively grounded MV distribution system which contains one feeder, can be shown as in Fig. 1. R_0, L_0 and C_0 indicate per-unit-length zero-sequence resistance, inductance and capacitance, respectively; $\dot{I}_{C0_i}(i=1,2,...,N_f-1)$ is the equivalent zero-sequence capacitive current per-unit-length; $\dot{U}_0$ and $\dot{U}_f$ are the zero-sequence voltages at the bus and the fault point, respectively; R_f is the fault resistance; $\dot{I}_0$ and $\dot{I}_f$ represent the zero-sequence currents to the bus and through the fault point (for metallic ground fault, R_f=0 and $\dot{I}_f$ has the largest amplitude); N_f is the number of nodes on the feeder. To properly represent the distributed capacitive current, the number of the PI sections in Fig. 1 should be infinite, so the number of N_f is infinite.

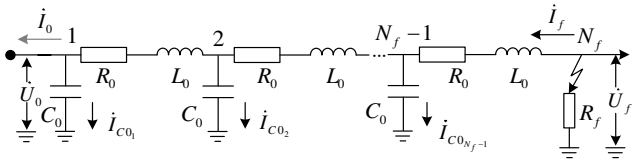

Fig. 1. Earth-fault zero-sequence network

The relationship between the zero-sequence voltage and current along the feeder can be represented as

$$\begin{bmatrix}\dot{U}_0\\ \dot{I}_0\end{bmatrix}=\begin{bmatrix}\cosh\gamma l & Z_c\sinh\gamma l\\ \dfrac{\sinh\gamma l}{Z_c} & \cosh\gamma l\end{bmatrix}^{-1}\begin{bmatrix}\dot{U}_f\\ \dot{I}_f\end{bmatrix} \tag{1}$$

where $Z_c=\sqrt{(R_0+j\omega L_0)/j\omega C_0}$ is the wave impedance; $\gamma=\sqrt{j\omega C_0R_0-\omega^2L_0C_0}$ is the transmission coefficient; and l is the length of the feeder. As there is only one feeder in the non-effectively grounded system, no other electrical components supply zero-sequence current to the bus bar. As a result, $\dot{I}_0$=0. For the fundamental frequency impedance of the distribution feeder, the resistance is comparable to the reactance. However, the frequency range of the dominated transient components during the fault is typically more than 200Hz [33, 34], in which the zero-sequence resistance is small with respect to the reactance. Thus, when considering the phase-frequency characteristics, the input zero-sequence impedance seen at the fault point can be represented as

$$Z_{oc}=\frac{\dot{U}_f}{\dot{I}_f}=Z_c\coth(l\gamma)\approx -j\sqrt{\frac{L_0}{C_0}}\cot\left(\omega l\sqrt{L_0C_0}\right) \tag{2}$$

where ω is the angular frequency.

The simplification is reasonable when the phase-frequency characteristics is investigated, as the resistance in the RLC circuit is related to the amplitude damping. It can be seen that the phase-frequency characteristics of Z_{oc} when R_0 is considered and ignored are only slightly different when series resonance and parallel resonance occur as shown in Fig. 2, where

$$\omega_k=\pi/2l\sqrt{L_0C_0} \tag{3}$$

Therefore, the influence of R_0 can be ignored when considering the phase-frequency characteristics of Z_{oc}.

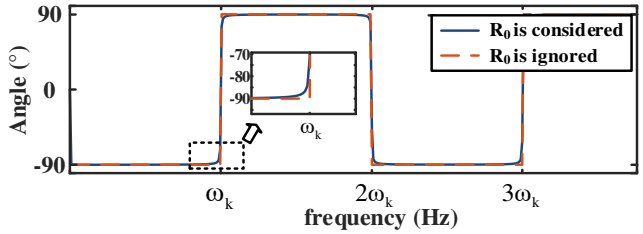

Fig. 2. Effect of R_0 on phase-frequency characteristics of Z_{oc}

Consequently, Z_{oc} is capacitive if

$$2n\omega_k < \omega < (2n+1)\omega_k \tag{4}$$

and is inductive if

$$(2n+1)\omega_k < \omega < 2n\omega_k \tag{5}$$

where $n = 0, 1, 2, ...$

The impedance of the equivalent circuit shows capacitive characteristic in the frequency range of $0 < \omega < \omega_k$, and then exhibits inductive and capacitive characteristics alternately with the increase of frequency in the range of $\omega > \omega_k$.

Based on the zero-sequence network of the neutral isolated system in Fig. 1, the zero-sequence network of the resonant grounded system is shown in Fig. 3. y_p is the zero-sequence admittance of the Peterson coil, and $\dot{U}_p$ is the zero-sequence voltage on the Peterson coil. The relationship between the voltage and current on the feeder can be represented as

$$\begin{bmatrix} \dot{U}_0 \\ \dot{I}_0 \end{bmatrix} = \begin{bmatrix} 1 & 0 \\ y_p & 0 \end{bmatrix} \begin{bmatrix} \dot{U}_p \\ 0 \end{bmatrix} \tag{6}$$

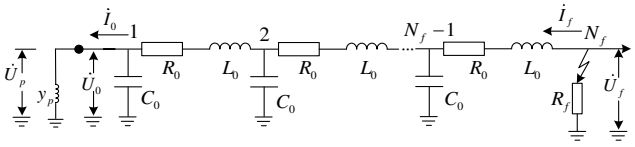

Fig. 3. Zero-sequence network of resonant grounded system

Combine (1) and (6), the input zero-sequence impedance Z_{oc}' in the resonant grounded system is expressed as

$$Z_{oc}' = Z_c \frac{\cosh(l\gamma) + y_p Z_c \sinh(l\gamma)}{\sinh(l\gamma) + y_p Z_c \cosh(l\gamma)} \tag{7}$$

Based on (2) and (7), the phase-frequency characteristics of the zero-sequence impedance of the neutral isolated system and the resonant grounded system are obtained, as shown in Fig. 3. For resonant grounded systems, the compensation range of the Peterson coil is [-10%, +10%], where "-" stands for under-compensation and "+" stands for over-compensation. Fig. 4 shows the phase-frequency characteristics of the zero-sequence impedance in the neutral isolated system, resonant grounded systems with 10% over-compensation and 10% under-compensation, respectively.

In Fig. 4, ω_0 is the fundamental frequency of the system, and C_p is the compensation degree of the Peterson coil. Due to the influence of the Peterson coil, the phase-frequency characteristics of the Z_{oc}' and Z_{oc} are slightly different around ω_0 and ω_k. Z_{oc}' is inductive in the full frequency band, and the bandwidth of this band is related to the inductance of the Peterson coil. Since the degree of compensation in the actual system is limited, parallel resonance occurs at about 1.8 times ω_0, as shown in Fig. 4①. The frequency at which the series resonance occurs for the first time is about ω_k, as shown in Fig.4②. As in the frequency that the equivalent circuit behaves inductive, the transient components will vanish quickly due to attenuation. So the transient signals in the frequency above ω_k is trivial but the noise could be severe. Therefore, the frequency range of the SFB in neutral ineffectively grounded system is chosen as $2\pi f_B < \omega < \omega_k$, where f_B is the boundary frequency and chosen as 200 Hz [33, 34].

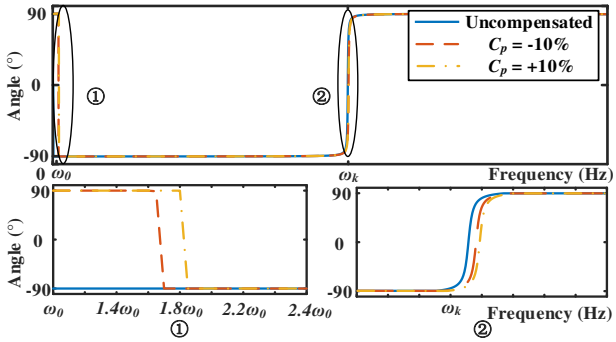

Fig. 4. Phase-frequency characteristics Considering the influence of Peterson coil

In the frequency range of the SFB, the zero-sequence voltage and zero-sequence fault current satisfy

$$ang\left(\frac{\dot{U}_f(\omega)}{\dot{I}_f(\omega)}\right) = -\frac{\pi}{2} \tag{8}$$

where ang is the function that calculates the phase angle of the phasor. And in the frequency range of $\omega > 0$, the voltages and the currents in the network except the fault point satisfy

$$ang\left(\frac{\dot{U}_{C_{0i}}(\omega)}{\dot{I}_{C_0 i}(\omega)}\right) = -\frac{\pi}{2}, i = 1, 2, ...N_f - 1 \tag{9}$$

where $\dot{U}_{C_{0i}}$ and $\dot{I}_{C_{0i}}$ represent the zero-sequence voltage and the zero-sequence capacitive current at node i.

The node with the maximum phase shift of the zero-sequence voltage is the one farthest from the fault point as shown in Fig. 1, hence the following equations hold:

$$\begin{cases} \max\left[ang\left(\dfrac{\dot{U}_f(\omega)}{\dot{U}_{C_{0i}}(\omega)}\right)\right] = ang\left(\dfrac{\dot{U}_f(\omega)}{\dot{U}_0(\omega)}\right) \\ \dot{U}_0 = \dfrac{\dot{U}_f}{\cosh \gamma_0 l} \end{cases} \tag{10}$$

The phase shift of the $\dot{U}_0(\omega)$ with the increase of frequency is shown in Fig.5(a). In the frequency range of $0 < \omega < \omega_s$, the phase shift is 0. The boundary frequencies ω_s and ω_k are equal, and the variation trend with the increase of l is shown in Fig.5(b).

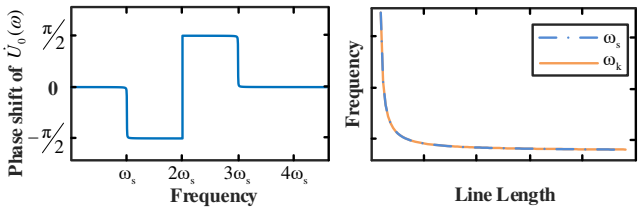

(a) Phase shift with frequency changes (b) ω_s with different line length

Fig. 5. Phase shift of zero-sequence voltage

Therefore, in the frequency range of the SFB, there is no phase shift between the zero-sequence voltages in the zero-sequence network. Furthermore, the phase of $\dot{I}_{C_{0i}}(\omega)$ and $\dot{I}_f(\omega)$ are equal within the SFB. Therefore, the amplitudes of $\dot{I}_{C_{0i}}(\omega)$ and $\dot{I}_f(\omega)$ satisfy:

$$I_f(\omega) = \sum_{i=1}^{N_f-1} I_{C_{0i}}(\omega) \tag{11}$$

As a result, in the frequency range of the SFB, the amplitudes of $\dot{I}_{C_{0i}}(\omega)$ and $\dot{I}_f(\omega)$ satisfy:

$$\int_{\omega\in SFB} I_f(\omega) = \sum_{i=1}^{N_f-1} \int_{\omega\in SFB} I_{C_{0i}}(\omega) \tag{12}$$

which means that the amplitudes of the fault current equals to the summation of the capacitive current within the SFB.

B. The SFB for a general MV network

The topology of the zero-sequence network of a general MV distribution network with lateral branches and DGs is shown in Fig. 6. In order to clarify the simplification process of the zero-sequence network, the equivalent circuit is presented as in Fig. 7(a). The circuit comprises a series of the basic unit as in the dotted box, which can be equivalent to the network shown in Fig. 7(b).

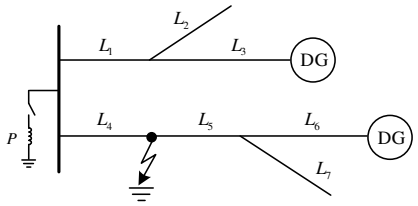

Fig. 6. The topology of the zero-sequence network

The equation of the equivalent circuit unit is

$$\begin{bmatrix}\dot{U}_{L_1}\\ \dot{I}_{L_1}\end{bmatrix} = \begin{bmatrix}\cosh\gamma l_1 & Z_c\sinh\gamma l_1\\ \dfrac{\sinh\gamma l_1}{Z_c} & \cosh\gamma l_1\end{bmatrix}\cdot\begin{bmatrix}1/2 & 0\\ 0 & 1\end{bmatrix}\cdot \left\{\begin{bmatrix}\cosh\gamma l_2 & Z_c\sinh\gamma l_2\\ \dfrac{\sinh\gamma l_2}{Z_c} & \cosh\gamma l_2\end{bmatrix}\begin{bmatrix}\dot{U}_{L_2}\\ 0\end{bmatrix} + \begin{bmatrix}\cosh\gamma l_3 & Z_c\sinh\gamma l_3\\ \dfrac{\sinh\gamma l_3}{Z_c} & \cosh\gamma l_3\end{bmatrix}\begin{bmatrix}\dot{U}_{L_3}\\ 0\end{bmatrix}\right\} \tag{13}$$

where l_i is the length of L_i, u_{L_1} and i_{L_1} indicate the transient zero-sequence voltage and current at the beginning of the line L_1; u_{L_2} (u_{L_3}) and i_{L_2} (i_{L_3}) represent the transient zero-sequence voltage and current at the end of the line L_2 (L_3).

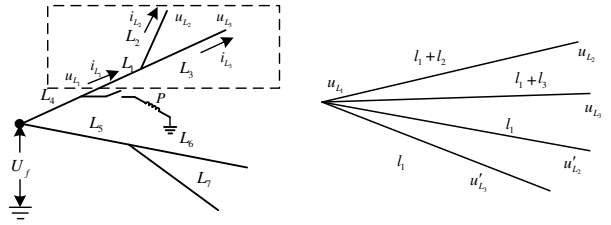

(a) The zero-sequence network (b) The equivalent circuit unit

Fig. 7. Zero-sequence network and the transformation

Set

$$\begin{bmatrix}1/(n+1) & 0\\ 0 & 1\end{bmatrix} = \begin{bmatrix}1 & 0\\ 0 & 1\end{bmatrix} + \begin{bmatrix}-n/(n+1) & 0\\ 0 & 0\end{bmatrix} \tag{14}$$

(13) can be converted into

$$\begin{aligned}\begin{bmatrix}\dot{U}_{L_1}\\ \dot{I}_{L_1}\end{bmatrix} &= \begin{bmatrix}\cosh\gamma(l_1+l_2) & Z_c\sinh\gamma(l_1+l_2)\\ \dfrac{\sinh\gamma(l_1+l_2)}{Z_c} & \cosh\gamma(l_1+l_2)\end{bmatrix}\begin{bmatrix}\dot{U}_{L_2}\\ 0\end{bmatrix}\\ &+ \begin{bmatrix}\cosh\gamma(l_1+l_3) & Z_c\sinh\gamma(l_1+l_3)\\ \dfrac{\sinh\gamma(l_1+l_3)}{Z_c} & \cosh\gamma(l_1+l_3)\end{bmatrix}\begin{bmatrix}\dot{U}_{L_3}\\ 0\end{bmatrix}\\ &+ \begin{bmatrix}\cosh\gamma l_1 & Z_c\sinh\gamma l_1\\ \dfrac{\sinh\gamma l_1}{Z_c} & \cosh\gamma l_1\end{bmatrix}\begin{bmatrix}\dot{U}'_{L_2}\\ 0\end{bmatrix} + \begin{bmatrix}\cosh\gamma l_1 & Z_c\sinh\gamma l_1\\ \dfrac{\sinh\gamma l_1}{Z_c} & \cosh\gamma l_1\end{bmatrix}\begin{bmatrix}\dot{U}'_{L_3}\\ 0\end{bmatrix}\end{aligned} \tag{15}$$

where

$$\dot{U}'_{L_2} = \frac{-\cosh\gamma_0 l_2}{2}\dot{U}_{L_2} \tag{16}$$

$$\dot{U}'_{L_3} = \frac{-\cosh\gamma_0 l_3}{2}\dot{U}_{L_3} \tag{17}$$

After four successive transformations as above, the topology of the zero-sequence network can be transformed to the equivalent network, as shown in Fig. 8. u_P indicates the transient zero-sequence voltage at the Peterson coil connection point; u_{L_6} (u_{L_7}) and i_{L_6} (i_{L_7}) are the transient zero-sequence voltage and current at the end of the line L_6 (L_7), respectively; and l_i is the length of the i^{th} line section.

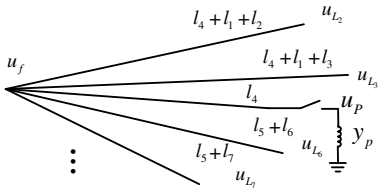

Fig. 8. The equivalent topology of the zero-sequence network

Therefore, considering the phase-frequency characteristics of the network, a general distribution network can be regarded as $2n+1$ lines connected in parallel, n is the number of the T node with branches. As a result, the phase-frequency characteristics of the distribution network is the same as the characteristics of the equivalent network as shown in Fig. 8. The frequency range of the SFB for neutral non-effectively grounded system is $2\pi f_B < \omega < \omega_k$. ω_k is determined by the longest line in the equivalent network, which can be calculated via (3).

III. The Scheme for Locating the Faulty Line section Based on D-PMUs

A. Fault section location criterion based on transient energy of the zero-sequence current within the SFB

Assume that there are *N* nodes in a distribution network and the D-PMUs are installed in the downstream of several nodes, the network is divided into *M* sections. When a single phase to ground fault occurs in the line section *F*, the relation of the zero-sequence current between faulty line section and healthy line sections within the frequency range of the SFB can be represented as

$$\begin{cases} \left|i_{S,F}^{(SFB)}\right| = \sum_{j\in M, j\neq F} \left|i_{S,j}^{(SFB)}\right| \\ i_{S,F}^{(SFB)} = -\sum_{j\in M, j\neq F} i_{S,j}^{(SFB)} \end{cases}, \ j = 1,2,...M \tag{18}$$

where $i_{S,j}^{(SFB)} = i_{upstream,j}^{(SFB)} - \sum i_{downstream,j}^{(SFB)}$ is the SFB component of the transient zero-sequence current difference between that flowing in and out the line section *j*; $i_{upstream,j}^{(SFB)}$ and $i_{downstream,j}^{(SFB)}$ are the SFB components of transient zero-sequence current, which can be monitored with the D-PMUs deployed at the upstream node and downstream nodes of the line section *j*.

Denote the transient energy in line section *j* as:

$$E_{SFB,j} = \int_0^{TF} \left[i_{S,j}^{(SFB)}(t) \right]^2 dt \tag{19}$$

where *TF* is the duration of the fault transient process. Then, an index for faulty line section identification is defined as

$$FLSI = (\max_{j\in M} E_{SFB,j}) \Big/ \left(\sum_{j\in M} E_{SFB,j} - \max_{j\in M} E_{SFB,j} \right) \tag{20}$$

According to (18), when the fault occurs in the line section *F*, the relation of the SFB components between healthy line sections and faulty line section can be expressed as

$$\left|i_{S,F}^{(SFB)}\right|^2 = \left(\sum_{j\in M, j\neq F} \left|i_{S,j}^{(SFB)}\right| \right)^2 \tag{21}$$

Therefore, the following in-equation holds for the instantaneous data obtained with the D-PMUs

$$\left(i_{S,F}^{(SFB)}\right)^2 \geq \sum_{j\in M, j\neq F} \left(i_{S,j}^{(SFB)}\right)^2 \tag{22}$$

And in the transient process after the fault, it holds that

$$\int_0^{TF} \left[i_{S,F}^{(SFB)}(t) \right]^2 dt > \sum_{j\in M, j\neq F} \int_0^{TF} \left[i_{S,j}^{(SFB)}(t) \right]^2 dt \tag{23}$$

As a result, when a single phase to ground fault occurs in line section F, the correspondent $FLSI$ is greater than 1.

But if the length of one line section is almost equal to the sum length of the rest line sections, $FLSI$ may still be greater than 1 when the fault occurs at the substation bus bar. In order to avoid the misjudgment, an auxiliary criterion is added:

$$SGN = \mathrm{sgn}\left(\int_0^{TF} \left[i_{S,F}^{(SFB)}(t) \cdot \sum_{j\in M, j\neq F} i_{S,j}^{(SFB)}(t) \right] dt \right) \tag{24}$$

where sgn is a function for calculating numeric symbols.

According to (18), when the fault occurs in the line section *F*, *SGN* is -1. Therefore, the necessary and sufficient conditions that indicate the fault occurs in the line section *F* can be expressed as follows

$$\begin{cases} FLSI > 1 \\ SGN = -1 \end{cases} \tag{25}$$

Otherwise, the fault occurs at the substation bus if $SGN = 1$.

B. The implementation procedures of the proposed scheme

The flow chart of the faulty line section location scheme is shown in Fig. 9, which includes the following steps:

1) Determination of the SFB. Based on the topology of the zero-sequence network, the maximum length of the equivalent line L_{LONG} is calculated, then ω_k is estimated by

$$\omega_k = \pi / 2L_{LONG}\sqrt{L_0 C_0} \tag{26}$$

where L_0 and C_0 denote per-unit-length zero-sequence inductance and capacitance of the network. And the frequency range of the SFB can be determined as in the range of 200 Hz to $\omega_k/2\pi$.

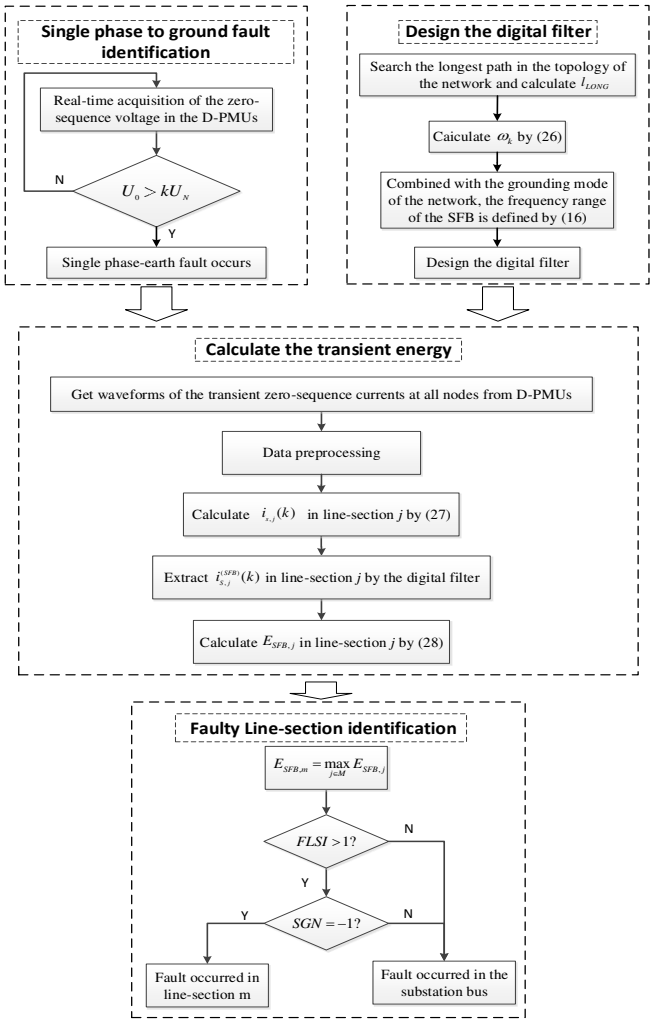

Fig. 9. Flow chart of the proposed fault location scheme

2) Single phase to ground fault detection. The instantaneous value of zero-sequence voltage acquired by the D-PMUs is monitored, the fault is considered detected if it is greater than the threshold kU_N, where U_N is the rated voltage and *k* is in the range of 0.05 ~ 0.10.

3) Transient energy calculation. The waveforms of the zero-

sequence currents during the fault are obtained by D-PMUs and uploaded to the distribution control center. Before being used for fault location, the data is preprocessed to eliminate the impact of outliers in the data. For each sampling point k, the instantaneous current difference $i_{S,j}(k)$ can be obtained as

$$i_{S,j}(k) = i_{upstream,j}(k) - \sum i_{downstream,j}(k) \tag{27}$$

$i_{S,j}(k)$ can also be seen as the zero-sequence current flowing to the earth from line section j ($j \in M$). And the concerned component $i_{S,j}^{(SFB)}(k)$ of line section j is extracted by a digital filter according to the value of the SFB. Then the transient energy in line section j is calculated by

$$E_{SFB,j} = \sum_{k=1}^{N} \left[i_{S,j}^{(SFB)}(k) \right]^2 \tag{28}$$

4) Faulty line section identification. The maximum of $E_{SFB,j}$ is calculated by

$$E_{SFB,m} = \max_{j \in M} E_{SFB,j} \tag{29}$$

And the fault occurs in the line section m if it satisfies

$$\begin{cases} FLSI = E_{SFB,m} \Big/ \sum_{j \in M, j \neq m} E_{SFB,j} > 1 \\ SGN = \operatorname{sgn}\left[\sum_{k=1}^{N} \left(i_{S,m}^{(SFB)}(k) \cdot \sum_{j \in M, j \neq m} i_{S,j}^{(SFB)}(k) \right) \right] = -1 \end{cases} \tag{30}$$

For the distribution networks including several feeders, the proposed method can be used to determine the faulty feeder and the faulty line section simultaneously.

IV. Case Study

A. Simulation Test

The IEEE 34 node distribution benchmark network is used to verify the proposed scheme, which is modeled and modified with PSCAD/EMTDC software. All loads are three-phase balanced constant power loads. There are five DGs in the network. Three photovoltaic power stations are connected to node 822, node 826 and node 848, of which the power supplies are 0.15MW, 0.3MW and 0.2MW. Two wind generators are added in node 838 and node 856, of which the power supplies are 0.3MW and 0.2MW. 16 D-PMUs are supposed randomly installed along the primary feeder buses as shown in Fig. 10. The sampling frequency is set as 10 kHz.

A single phase to ground fault is set to occur at k3, which is 22.57 km away from the bus bar. Table I shows the results of different situations with different initial angles (F_θ), grounding resistance (F_R), and SNR. The proposed scheme is tested using the fault scenarios listed in Table I. All the faulty line section location results are correct, which show the proposed method suitable for the faults in different initial angles and grounding resistances. Fault *Case A*, as in the bolded line in Table I, is taken as an example to illustrate the results in detail. Fig. 11(a) and Fig. 11(b) are the original and polluted transient zero-sequence currents, respectively. The SFB components are extracted, which is shown in Fig. 11(c). And the transient energy distribution of all line sections is shown in Fig. 11(d), which give a good discrimination degree between healthy line sections and faulty line section.

Table II shows the faulty line section detection results for different faulty line sections and faulty distance from the bus. The initial phase angle, fault resistance, fault phase and SNR is 0°, 0Ω, phase A and 5dB, respectively. The bold line of Table II, named *Case B* that the fault occurs at the bus, is taken as an example to illustrate the results. The transient energy is shown in Fig. 12, and there is no obvious difference between the transient energy of different line sections. The fault at the bus bar is also located correctly. It can be seen from Table II that the method can achieve faulty line section identification in various faulty distances, even for those at the bus bar, at the end of the line as well as the laterals connected to T nodes.

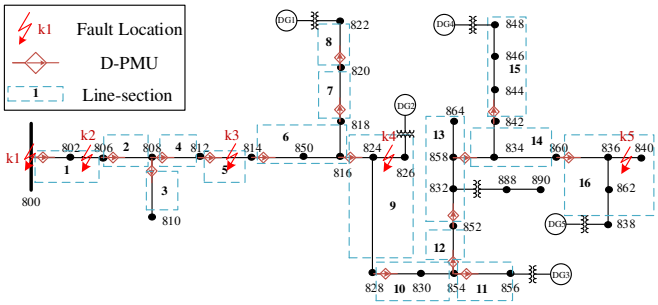

Fig. 10. Single-line diagram of IEEE-34 system

TABLE I
LOCATION RESULTS FOR DIFFERENT F_θ AND F_R

Faulty Line Section	F_θ (°)	F_R (Ω)	SNR (dB)	*FLSI*	*SGN*	Location Results
5	0	0	5	9.26	-1	5
	0	0	-1	9.15	-1	5
	0	50	5	8.92	-1	5
	0	500	5	9.05	-1	5
	0	**500**	**-1**	**9.31**	**-1**	**5**
	60	0	5	8.73	-1	5
	90	0	5	9.17	-1	5

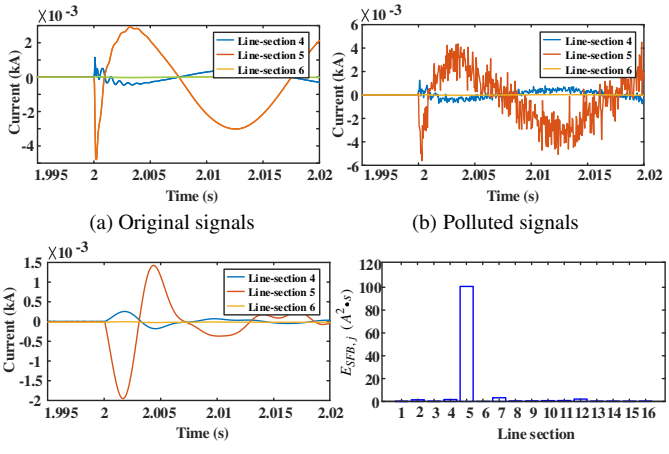

(a) Original signals (b) Polluted signals

(c) SFB components (d) Transient energy distribution

Fig. 11. Signals and transient energy distribution of Case A

The influence of DG is also taken into consideration. When a single phase to ground fault occurs at k3, the initial phase angle, fault resistance, fault phase and SNR is 0°, 0Ω, phase A and 5dB. Table III shows the faulty line detection results for different allocation of DGs. Table IV shows the faulty line detection results for different power injected by the DGs. In

Table IV, there is no change in Test Number 1. The power supply of DG3 is changed to 0.1MW and 0.5MW in Test Number 2 and Test Number 3. In the Test Number 4, the power supply of DG4 is changed to 0.4MW. In the Test Number 5, the power supply of DG3 and DG4 is changed to 0.1MW and 0.4MW. The proposed method can determine the fault line sections for different allocation of DGs and different power injected by the DGs.

Table V shows the faulty line detection results for different compensation degrees (C_p) of the Peterson coil. It shows that fault line sections can be correctly identified in a wide compensation range.

The effect of different load type is evaluated, as shown in Table VI. When a single phase to ground fault occurs at k5, the initial phase angle, fault resistance, fault phase and SNR is 0°, 0Ω, phase A and 5dB. The load conditions considered in Test Number 1 is that all loads are three-phase balanced constant power loads. In Test Number 2, the loads connected to node 836, node 838, node 840, and node 860 are removed. In Test Number 3, the load connected to the node 836 is changed to a two-phase constant power load, and the loads connected to the node 838, node 840 and node 860 are changed to one-phase constant power loads. In Test Number 4, the loads connected to the node 836 and node 840 are changed to three-phase balanced nonlinear power loads. According to the fault location results in Table VI, it can be seen that there is no influence on the FLSI and the fault location results for different load types.

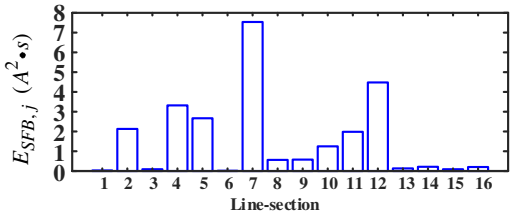

Fig. 12. Transient energy distribution of Case B

TABLE II
LOCATION RESULTS FOR DIFFERENT LINE SECTIONS

Faulty Line Section	Distance (km)	*FLSI*	*SGN*	Location Results
bus bar	**0**	**0.424**	**1**	**bus bar**
1	0.79	9.73	-1	1
5	22.57	9.13	-1	5
9	35.76	8.91	-1	9
16	57.68	8.77	-1	16

TABLE III
LOCATION RESULTS FOR DIFFERENT ALLOCATION OF DGS

Faulty Line Section	Allocation of DGs	*FLSI*	*SGN*	Location Results
5	DG1~DG5	9.37	-1	5
	DG2~DG5	9.52	-1	5
9	DG1~DG5	9.08	-1	9
	DG2~DG5	9.44	-1	9

TABLE IV
LOCATION RESULTS FOR DIFFERENT POWER INJECTED BY THE DGS

Number	Faulty Line Section	DGs' Power Adjustment	*FLSI*	*SGN*	Location Results
1	5	No change	9.11	-1	5
2		0.1 MW (DG3)	8.72	-1	5
3		0.5 MW (DG3)	9.03	-1	5
4		0.4 MW (DG4)	8.79	-1	5
5		0.1 MW (DG3) and 0.4 MW (DG4)	9.08	-1	5

TABLE V
LOCATION RESULTS FOR RESONANT GROUNDED SYSTEM WITH DIFFERENT COMPENSATION RATE

Faulty Line section	C_p (%)	*FLSI*	*SGN*	Location Results
5	-8	9.88	-1	5
	-5	9.84	-1	5
	5	9.72	-1	5
	8	9.81	-1	5

TABLE VI
LOCATION RESULTS FOR DIFFERENT LOADS

Number	Faulty Line Section	Load Condition	*FLSI*	*SGN*	Location Results
1	16	No change	9.08	-1	16
2		Loads removed	8.83	-1	16
3		Unbalanced Loads	8.93	-1	16
4		Nonlinear Loads	9.11	-1	16

When analyzing the robustness to measurement, the influence of noise and outliers have been taken into consideration. When SNR is -1dB, the fault location can still be accurately located as shown in Table I, which proves that the method has good noise immunity. The impact of the outliers also has been analyzed. When a single phase to ground fault occurs at k3, the initial phase angle, fault resistance, fault phase and SNR is 0°, 0Ω, phase A and 5dB. The results are presented in Table VII. There is no bad data for Test Number 1. In Test Number 2, part of the data measured at node 806 is lost during transmission, and part of the data measured at node 828 has impulse noise in Test Number 3. In Test Number 4, part of the data measured at node 814 during transmission is lost, and part of the data measured at node 860 has impulse noise. Taking Test Number 4 in Table VII as *Case C*, the original waveform, the polluted waveform and the corrected waveform of the signals measured at node 814 and node 860 are as shown in Fig. 13(a) and Fig. 13(b). The transient energy distribution of the system is as shown in Fig. 13(c). Comparing the corrected waveform with the original waveform, it is seen that the outliers can be effectively corrected by using the robust local regression smoothing filtering method [35]. Using the corrected signals, the transient energy of each line section are calculated and the faulty line section can be accurately located. After the data preprocessing, the outliers will not affect the location results.

TABLE VII
LOCATION RESULTS WITH OUTLIERS

Number	Faulty Line Section	Outliers	*FLSI*	*SGN*	Location Results
1	5	No Outliers	9.15	-1	5
2		Impulse Noise	8.67	-1	5
3		Lost Data	8.88	-1	5
4		**Impulse Noise and Lost Data**	**9.10**	**-1**	**5**

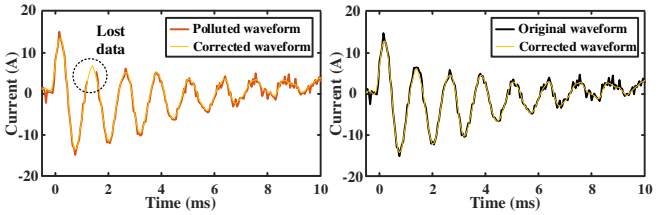

(a) Original waveform, polluted waveform and corrected waveform (node 814)

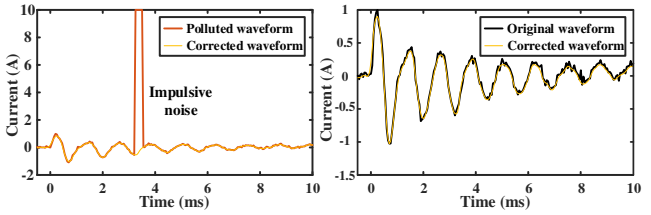

(b) Original waveform, polluted waveform and corrected waveform (node 860)

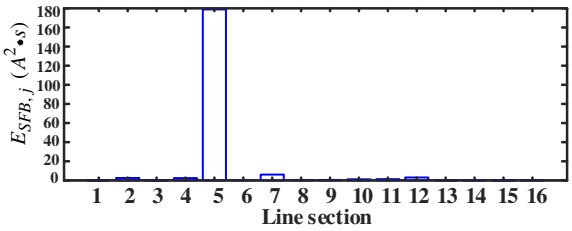

(c) Transient energy distribution

Fig. 13. Signals and transient energy distribution of Case C

The robustness to parameter uncertainty is also discussed. According to the parameters given by the system, the frequency range of the SFB is calculated to be 200-770Hz, and the parameters of the system are changed but the SFB is not recalculated. When a single phase to ground fault occurs at k3, the initial phase angle, fault resistance, fault phase and SNR is 0°, 0Ω, phase A and 5dB. There is no change in the parameters of the line in Test Number 1. In Test Number 2 and Test Number 3, the line resistance of the entire system was set to 80% and 120% of the original resistance. In Test Number 4 and Test Number 5, the line inductance of the entire system was set to 80% and 120% of the original inductance. In Test Number 6 and Test Number 7, the shunt capacitance of the entire system was set to 80% and 120% of the original capacitance. The results are presented in Table VIII. According to the location results in the Table VIII, it can be seen that there is no influence on the *FLSI* and the results when any parameter of the entire network line changes by 20%.

TABLE VIII
LOCATION RESULTS WITH DIFFERENT PARAMETERS

Number	Faulty Line Section	Parameters	*FLSI*	*SGN*	Location Results
1		No change	9.17	-1	5
2		80% resistance	8.95	-1	5
3		120% resistance	8.98	-1	5
4	5	80% inductance	7.21	-1	5
5		**120% inductance**	9.18	**-1**	**5**
6		80% capacitance	9.57	-1	5
7		120% capacitance	9.01	-1	5

B. *On field fault experiments test*

We carried out on field test at a real 10kV distribution network in China, the structure of the network is shown in Fig. 14. The transformer is 0.4/10kV with Y-delta connection, and the neutral point of the grounding transformer has two working modes: ungrounded or via the Peterson coil. There are five feeders, including cable, overhead line and hybrid feeder. Arc suppression coil is WZXC-1000/10.5, the parameters are as follows: rated capacity 1000kvar, rated current 165A, rated frequency 50Hz. The parameters of the grounding transformer are as follows: rated capacity 1200/200kVA, rated voltage 10.5±2×2.5%/0.4kV, rated current 65.98/288.68A, neutral current 165 A, rated frequency 50Hz. The D-PMUs are deployed at the beginning of all the feeders and a D-PMU is installed at the junction of the overhead line and the cable in feeder 2. The sampling frequency of the D-PMUs is 200 points per cycle. In the test, the fault location procedure is triggered according to the zero-sequence voltage at the bus. Whether it is a bus bar fault or a line fault is firstly identified and then the faulty line section is located via (30).

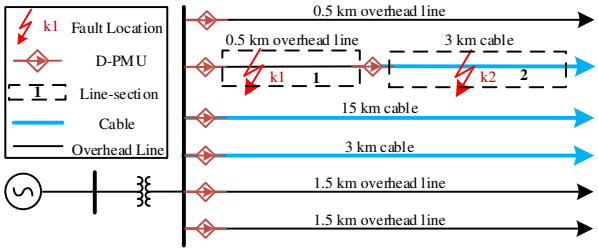

Fig. 14. The structure of the 10kV network for fault experiment

A various of single phase to ground fault experiments are implemented on feeder 2, including different neutral grounded mode, different grounding resistance and different compensation degree. Fault occurs at k1 on the overhead line of feeder 2 and k2 on the cable of feeder 2. k1 is 150 m away from the bus, and k2 is 600 m away from the bus. Some photos of the on-field fault experiments are shown in Fig. 15. The faulty feeder selection and the faulty line section location are implemented separately. The results are presented in Table IX. Taking *Case D*, as in the bolded line in Table IX, as an example to illustrate the effectiveness of the proposed method in real system, Fig. 16 shows the related waveform for *Case D*. Fig. 16(a) and Fig. 16(b) are the original transient zero-sequence currents and the SFB components, respectively. Transient energy of every line and every line section is shown in Fig. 16(c). The transient energy of faulty line is larger than the transient energy of other lines, and the transient energy of faulty line section is larger than the transient energy of other line sections, so the faulty feeder and faulty line section can be identified based on the transient energy. The fault location results in Table IX are correct, which indicates that the proposed scheme can detect faulty line section effectively in radiation network including several feeders.

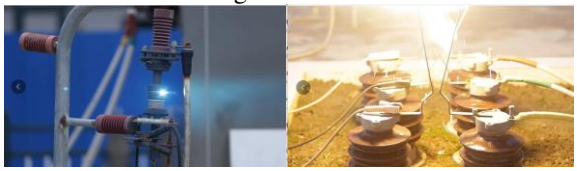

Fig. 15. The on-field single phase to ground fault experiments

TABLE IX
LOCATION RESULTS OF FIELD TEST

Fault Location	Neutral Grounding Mode	R_f	Faulty Feeder Selection		Results (Faulty Feeder)	Faulty Line Section Detection	Results (Faulty Line Section)
			FLSI	*SGN*		*FLSI*	
k1	Ungrounded	0	2.01	-1	2	48.75	1
		125	1.72	-1	2	59.65	1
		500	1.68	-1	2	4.33	1
		1000	1.59	-1	2	4.31	1
		2000	1.54	-1	2	3.57	1
	Resonant grounded (Over-compensation)	0	1.81	-1	2	11815.85	1
		125	1.72	-1	2	42978.17	1
		500	1.37	-1	2	92.87	1
		1000	1.95	-1	2	1.21	1
		2000	1.46	-1	2	1.44	1
k2	Ungrounded	0	3.46	-1	2	1087.65	2
		167	2.48	-1	2	897.33	2
		500	2.56	-1	2	778.50	2
		1000	2.88	-1	2	411.22	2
		2000	1.99	-1	2	312.45	2
	Resonant grounded (Over-compensation)	**0**	**1.81**	**-1**	**2**	**635.89**	**2**
		167	1.79	-1	2	418.95	2
		500	1.52	-1	2	107.18	2
		1000	1.88	-1	2	23.06	2
		2000	1.54	-1	2	2.59	2
	Resonant grounded (Under-compensation)	0	1.83	-1	2	570.49	2
		167	1.95	-1	2	1543.84	2
		500	2.03	-1	2	899.74	2
		1000	2.25	-1	2	11.89	2
		2000	2.15	-1	2	2.51	2

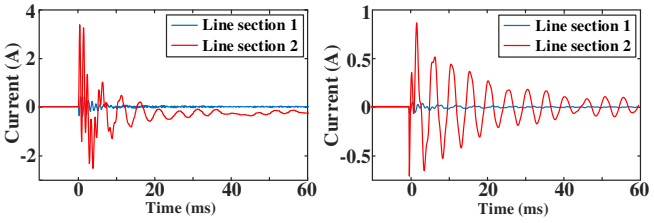

(a) Original signals (b) SFB components

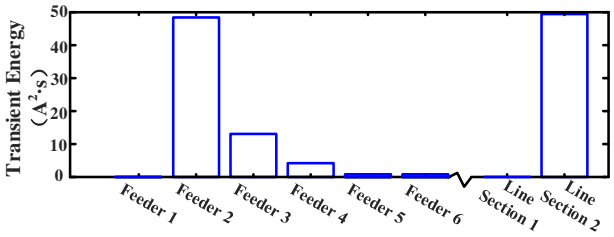

(c) Transient energy of Case D

Fig. 16. Signals and transient energy of Case D

V. COMPARISON WITH OTHER METHODS

In order to present the reliability advantage of faulty line section identification method with strong noise background, we compared this method with three methods introduced in [12], [36] and [16], which have been verified in distribution network and are denoted as Method A, B and C, respectively.

Method A: It uses the amplitude and phase of the zero-sequence admittance of the line section to identify the faulty line section, and the zero-sequence admittance is obtained by dividing zero-sequence current and zero-sequence voltage.

The comparison of identification accuracy for Method A and the proposed method in different conditions is shown in Table X. In Table X (a), the fault conditions of SNR and initial phase angle are 20 dB and 0°, respectively. In Table X (b), the fault scenarios of SNR, initial phase angle and grounding resistance are 20 dB, 0° and 5 Ω, respectively. In order to verify the noise immunity of the method, each group of the simulations was repeated 1000 times with random noises.

TABLE X

(a) Accuracy Comparison for Different Location and F_R

Faulty Line section	F_R (Ω)	Accuracy of Method A	Accuracy of the proposed Method
5	0	100%	100%
	500	100%	100%
16	0	100%	100%
	500	100%	100%

(b) Accuracy Comparison for Different Location and C_P

Faulty Line section	C_P (%)	Accuracy of Method A	Accuracy of the proposed Method
5	5	97.1%	100%
	8	97.2%	100%
16	**5**	**66.1%**	**100%**
	8	64.9%	100%

The results show that Method A and the proposed method both correctly detect the single phase-earth fault line section in the neutral isolated system. But Method A produces some misjudgments in resonant grounded system, especially when the fault is at the end of the line. The reason is that the steady state zero-sequence current is weak in resonant grounded system, the weak steady-state zero-sequence current is disturbed and the phase of the zero-sequence admittance has large errors. The bold part of Table X(b) is taken as an example, and 1 group phasors of zero-sequence admittance based on Method A are shown in Fig.17, which indicate that the noises lead to large errors in the phase of zero-sequence admittance. The proposed method is immune to strong noises.

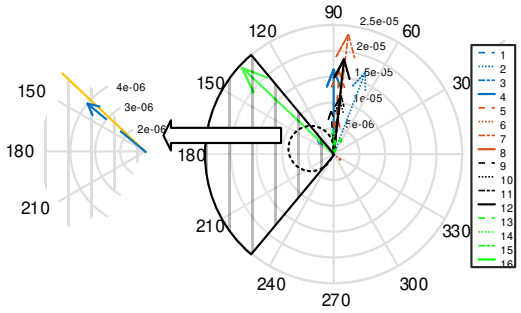

Fig. 17. Phasors of Zero-sequence Admittance

Method B: It uses the corrected correlation coefficient (C_{cor}) of the transient zero-sequence currents to identify the faulty line section, of which the threshold is 0.5. However, Method B is not suitable for some scenarios. Using the benchmark network shown in Fig. 10, more D-PMUs are deployed in the node 810, node 822, node 856, node 848 and node 840. The

faulty conditions of SNR, initial phase angle and grounding resistance are 20 dB, 0° and 5 Ω .

As shown in Table XI, method B is completely ineffective because the zero-sequence current near the substation bus bar and the end of the line. Meanwhile, the proposed method can determine the faulty line section correctly. Compared with method B, the proposed method is suitable for more fault scenarios, and needs less measuring equipment.

TABLE XI
LOCATION RESULTS OF METHOD B

Fault Location	C_{cor}	True or False
k2	[**0.0223**, 0.8492, **-0.0297**, 0.8353, 0.8597, (0.7534, 0.6224), 0.9448, **0.0169**, 0.9533, (0.8336, 0.8872), **0.0088**, 0.9440, 0.9935, (0.9912, 0.9920), **0.0192**, **-0.0035**]	False
k3	[**0.0248**, 0.9466, **-0.0222**, 0.9028, **-0.2986**, (0.5926, 0.3955), 0.9107, **0.0090**, 0.9151, (0.6823, 0.7832), **-0.0240**, 0.8839, 0.9863, (0.9812, 0.9829), **0.0126**, **-0.0201**]	False
k4	[**0.0572**, 0.9177, **0.0368**, 0.8322, 0.8291, (0.5457, -0.5983), 0.8288, **-0.0252**, **-0.4980**, (0.6027, 0.7557), **0.0311**, 0.8457, 0.9802, (0.9716, 0.9742), **0.0240**, **-0.0332**]	False
k5	[**0.0133**, 0.9691, **0.0407**, 0.9316, 0.9239, (0.7803, -0.8273), 0.9371, **-0.0029**, 0.9396, (-0.5335, 0.8007), **0.0052**, 0.8152, 0.9594, (-0.2998, 0.9245), **0.0137**, **-0.0022**]	False

Method C: The protection criterion established by using the slope relation matrix can be applied to detect the faulty feeder of single phase to ground faults. The threshold is set equal to −0.5. The location results for Method C in different conditions are shown in Table XII using the field data in Table IX.

TABLE XII
LOCATION RESULTS OF METHOD C

Fault Location	Neutral Grounding Mode	R_f	λ_i [λ_1 λ_2 λ_3 λ_4 λ_5 λ_6]	Result
k1	Ungrounded	0	[0.16, **-1.82**, 0.55, 0.50, 0.56, 0.05]	Right
		125	[-0.01, -0.35, 0.05, 0.08, 0.14, 0.09]	False
		500	[0.19, **-0.54**, 0.19, 0.32, -0.20, 0.03]	Right
		1000	[-0.07, -0.05, -0.07, 0.05, -0.24, 0.37]	False
		2000	[0.02, -0.08, 0.27, -0.28, -0.05, 0.13]	False
	Over-compensation	0	[0.59, **-1.65**, 0.37, 0.34, 0.05, 0.29]	Right
		125	[0.25, **-1.12**, 0.05, 0.30, 0.34, 0.19]	Right
		500	[-0.01, -0.14, -0.04, -0.01, 0.05, 0.15]	False
		1000	[0.08, 0.00, -0.09, 0.17, 0.05, -0.22]	False
		2000	[0.16, -0.30, -0.14, 0.21, 0.04, 0.03]	False
k2	Ungrounded	0	[0.65, **-1.23**, 0.10, 0.16, 0.53, -0.21]	Right
		167	[0.22, -0.26, 0.09, 0.17, 0.07, -0.29]	False
		500	[0.29, **-0.80**, 0.08, 0.21, -0.06, 0.30]	Right
		1000	[0.17, -0.26, 0.25, 0.13, -0.11, -0.18]	False
		2000	[0.10, -0.33, 0.06, 0.07, -0.01, 0.12]	False
	Over-compensation	**0**	[0.64, **-1.77**, 0.47, 0.41, 0.43, -0.18]	Right
		167	[0.30, **-0.57**, 0.17, 0.18, -0.31, 0.23]	Right
		500	[0.11, 0.06, -0.18, -0.03, 0.04, 0.00]	False
		1000	[-0.04, -0.11, 0.13, -0.03, -0.00, 0.07]	False
		2000	[0.35, -0.13, **-0.59**, 0.23, 0.10, 0.04]	False
	Under-compensation	0	[0.58, **-1.76**, 0.62, 0.64, -0.26, 0.18]	Right
		167	[0.26, -0.32, 0.34, 0.34, 0.21, **-0.84**]	False
		500	[0.08, **-0.64**, 0.26, 0.37, 0.08, -0.15]	Right
		1000	[0.13, -0.26, 0.01, 0.13, -0.03, 0.02]	False
		2000	[0.21, -0.33, 0.32, -0.24, -0.06, 0.10]	False

Because the data processing method of Method A is not mentioned in [16], the results show that Method C can detect the faulty feeder if the grounding resistance is 0 Ω but it doesn't work properly sometime, especially when the grounding resistance is bigger than 200 Ω. The noise in the actual distribution grid is very strong, resulting in incorrect location results if the grounding resistance is large. The proposed method is more reliable in detecting the faulty feeder and identifying the faulty line section in the actual distribution network.

VI. CONCLUSIONS

This paper proposes an integrated technique based on the D-PMUs to identify the faulty line section for neutral non-effectively grounded MV networks. The paper investigates the determination of the SFB within which the transient energy of the monitored signal is far greater than the energy of the noise, the transient energy of faulty line section is proven to be greater than the energy of the healthy line sections. A method based on a combined criterion is proposed, and the implementation of the scheme is illustrated. Both the simulation and on-field fault experiment results show that the proposed method is not affected by strong background noise, fault locations, load types, grounding resistances, inception angles, locations and power supply of DGs. And the method is also robust to line parameters and outliers. Three methods are compared with the proposed method to prove that the proposed method is more accurate and applicable.

VII. EFERENCES

[1] S. Jamali and A. Bahmanyar, "A new fault location method for distribution networks using sparse measurements," *International Journal of Electrical Power & Energy Systems*, vol. 81, pp. 459-468, Oct. 2016.

[2] H. Chen, P. D. S. Assala, Y. Cai, and P. Yang, "Intelligent transient overvoltages location in distribution systems using wavelet packet decomposition and general regression neural networks," *IEEE Trans. Industrial Informatics*, vol. 12, no. 5, pp. 1726-1735, Oct. 2016.

[3] D. Topolanek, M. Lehtonen, M. R. Adzman and P. Toman, "Earth fault location based on evaluation of voltage sag at secondary side of medium voltage/low voltage transformers," *IET Gener. Transmission & Distribution*, vol. 9, no. 14, pp. 2069-2077, Nov. 2015.

[4] Y. Xue, L. Guo, L. Zhang, B. Xu and T. Li, "Selection Problems of Neutral Grounding Mode in Active Distribution Networks. Automation of Electric Power Systems," vol. 39, no. 13, pp. 129-126, May, 2015. (in Chinese)

[5] P. Liu and C. Huang, "Detecting single-phase-to-ground fault event and identifying faulty feeder in neutral ineffectively grounded distribution System," *IEEE Trans. Power Delivery*, vol. 33, no. 5, 2265-2273, Oct. 2018.

[6] D. Griffel, V. Leitloff, Y. Harmand and J. Bergeal, "A new deal for safety and quality on MV networks," *IEEE Trans. Power Delivery*, vol. 12, no. 4, pp. 1428-1433, Oct. 1997.

[7] Z. Zhang, Z. Wang, and K. Li, "The summarization of fault line selection of Small current grounding system," *International Symposium on Vehicle, Mechanical, and Electrical Engineering (ISVMEE)*, 21-22, Dec, 2013, pp. 1775-1778, Taiwan, China.

[8] F. Han, Y. Zhang, S. Hao, and X. Zhao, "Research on single-phase-to-earth fault location based on Hilbert-huang transform," *2016 IEEE Advanced Information Management, Communicates, Electronic and Automation Control Conference (IMCEC)*, 3-5 Oct. 2016, pp. 1338-1441, Xi'an, China.

[9] X. Zeng, K. Li, W. Chan, S. Su and Y. Wang, "Ground-Fault Feeder Detection With Fault-Current and Fault-Resistance Measurement in Mine Power Systems," *IEEE Trans. Industry Applications*, vol. 44, no. 2, pp. 424-429, Mar. 2008.

[10] X. Lin, J. Huang and S. Ke, "Faulty Feeder Detection and Fault Self-Extinguishing by Adaptive Petersen Coil Control," *IEEE Trans. Power Delivery*, vol. 26, no. 2, pp. 1290-1291, Apr. 2011.
[11] Z. Zhang, X. Liu and Z. Piao, "Fault line detection in neutral point ineffectively grounding power system based on phase-locked loop," *IET Gener. Transmission & Distribution*, vol. 8, no. 2, pp. 273-280, Feb. 2014.
[12] L. Zhang, H. Gao, B. Xu and Y. Xue, "Fault location method based on zero sequence admittance measurement in non-effectively earthed system," *IEEE PES Innovative Smart Grid Technologies*, Tianjin, 21-24 May 2012, pp. 1-4.
[13] X. Dong and S. Shi, "Identifying Single-Phase-to-Ground Fault Feeder in Neutral Noneffectively Grounded Distribution System Using Wavelet Transform," *IEEE Trans. Power Delivery*, vol. 23, no. 4, pp. 1829-1837, Oct. 2008.
[14] C. Zhou, Q. Shu and X. Han, "A single-phase earth fault location scheme for distribution feeder on the basis of the difference of zero mode traveling waves," *International Trans. on Electrical Energy Systems*, vol. 27, no. 5, pp. e2298.
[15] Y. Tao, and Y. Juan, "A Survey on Single-Phase Faulty Line Selection Techniques for Small Current Grounding System in Medium-voltage Grid," *Applied Mechanics and Materials*, vol. 492, pp. 407-411, Jan. 2014.
[16] Y. Wang, Y. Huang, X. Zeng, G. Wei, J. Zhou, T. Fang, and H. Chen, "Faulty feeder detection of single phase-earth fault using grey relation degree in resonant grounding system," *IEEE Trans. Power Delivery*, vol. 32, no. 1, pp. 55-61, Feb. 2017.
[17] Y. Fang, Y. Xue, H. Song, T. Guan, F. Yang and B. Xu, "Transient Energy Analysis and Faulty Feeder Identification Method of High Impedance Fault in the Resonant Grounding System". Proceedings of CSEE, vol. 38, no. 19, pp. 5636-5645, Oct. 2018. (in Chinese)
[18] X. Wang, J. Gao, M. Chen, X. Wei, Y. Wei and Z. Zeng, "Faulty Line Detection Method Based on Optimized Bistable System for Distribution Network," *IEEE Trans. on Industrial Informatics*, vol. 14, no. 4, pp. 1370-1381, Apr. 2018.
[19] M. Pourahmadi-Nakhli and A. A. Safavi, "Path Characteristic Frequency-Based Fault Locating in Radial Distribution Systems Using Wavelets and Neural Networks," *IEEE Trans. Power Delivery*, vol. 26, no. 2, pp. 772-781, Apr. 2011.
[20] X. Lin, J. Huang and S. Ke, "Faulty feeder detection and fault self-extinguishing by adaptive petersen coil control," *IEEE Trans. Power Delivery*, vol. 26, no. 2, pp. 1290-1291, Apr. 2011.
[21] W. Wang, K. Zhu, P. Zhang and W. Xu, "Identification of the Faulted Distribution Line Using Thyristor-Controlled Grounding," *IEEE Trans. Power Delivery*, vol. 24, no. 1, pp. 52-60, Jan. 2009.
[22] P. Wang, B. Chen, H. Zhou, T. Cuihua and B. Sun, "Fault Location in Resonant Grounded Network by Adaptive Control of Neutral-to-Earth Complex Impedance," *IEEE Trans. on Power Delivery*, vol. 33, no. 2, pp. 689-698, Apr. 2018.
[23] C. Huang, T. Tang, Y. Jiang, L. Hua and C. Hong, "Faulty feeder detection by adjusting the compensation degree of arc-suppression coil for distribution network," *IET Gener. Transmission & Distribution*, vol. 12, no. 4, pp. 807-814, Feb. 2018.
[24] X. Zeng, Y. Xu,, and Y. Wang, "Some novel techniques for insulation parameters measurement and Petersen-Coil control in distribution systems," *IEEE Trans. Industrial Electronics*, vol. 57, no. 4, pp. 1445-1451, Apr. 2010.
[25] P. Wang, B. Chen, H. Zhou, T. Cuihua and B. Sun, "Fault Location in Resonant Grounded Network by Adaptive Control of Neutral-to-Earth Complex Impedance," *IEEE Trans. Power Delivery*, vol. 33, no. 2, pp. 689-698, Apr. 2018.
[26] J. Zhou, and K. Cao, "Locating method of single-phase grounding fault in small current grounding system based on distribution automation," *International Conference on Mechatronics and Industrial Informatics (ICMII)*, Applied Mechanics and Materials, vol, 321, pp. 1423-1428, Jun. 2013.
[27] K. Jia, Z. Ren, L. Li, Z. Xuan and D. Thomas, "High-frequency transient comparison based fault location in distribution systems with DGs, " *IET Gener. Transmission & Distribution*, vol. 11, no. 16, pp. 4068-4077, Nov. 2017.
[28] K. Jia, C. Gu, T. Bi and D. Thomas, "Sparse Voltage Amplitude Measurement Based Fault Location in Large-Scale Photovoltaic Power Plants, " *Applied Energy*, vol. 211. pp. 568-581, Feb. 2018.
[29] H. Zhang, Z. Jin and Y. Liu, "Wide-area Measurement System Light and Its Application in China," Automation of Electric Power Systems, vol. 38, no. 22, pp. 85-90, Nov. 2014. (in Chinese)
[30] Z. Jin, H. Zhang and C. Li, "WAMS light and its deployment in China," *2015 5th International Conference on Electric Utility Deregulation and Restructuring and Power Technologies (DRPT)*, Changsha, 2015, pp. 1373-1376.
[31] A. v. Meier, E. Stewart, A. McEachern, M. Andersen, and L. Mehrmanesh, "Precision Micro-Synchrophasors for Distribution Systems: A Summary of Applications," *IEEE Transactions on Smart Grid*, vol. 8, no. 6, pp. 2926-2936, Nov. 2017.
[32] A. von Meier, D. Culler, A. McEachern, R. Arghandeh. "Micro-Synchrophasors for Distribution Systems," 2014 IEEE Pes Innovative Smart Grid Technologies Conference (ISGT), 19-22 Feb. 2014, Washington, DC, United states.
[33] Y. Xue, B. Xu, Y. Chen, Z. Feng, and P. Gale, "Earth fault protection using transient signals in non-solid earthed network," in Proceedings. International Conference on Power System Technology, 14-22 Feb. 2002, pp. 1763-1767, Kunming, China.
[34] M. F. Abdel-Fattah, M. J. J. o. E. Lehtonen, and P. Engineering, "A new transient impedance-based algorithm for earth fault detection in medium voltage networks," Journal of Energy and Power Engineering, vol. 6, no. 2, pp. 240-249, Jun. 2012.
[35] H. Zhang, Z. Jin and V. Terzija, "An Adaptive Decomposition Scheme for Wideband Signals of Power Systems Based on the Modified Robust Regression Smoothing and Chebyshev-II IIR Filter Bank," *IEEE Trans. Power Delivery*, vol. 34, no. 1, pp. 220-230, Feb. 2019.
[36] T. Li and C. Huang, "New transient fault location method in non-solidly earthed system for distribution network," *CIRED - Open Access Proceedings Journal,* vol. 2017, no. 1, pp. 1330-1333, Oct. 2017.

Xuewen Wang received B.E degree in electrical engineering from Shandong University. He is now a post-graduate student majoring in electrical engineering in Shandong University. His research interest includes fault location for distribution networks, power system simulation.

Fang Shi (M' 10) received the Ph.D. degree from Shanghai Jiao Tong University, Shanghai, China, 2014.
He is currently a lecturer in the Key Laboratory of Power System Intelligent Dispatch and Control of the Ministry of Education (Shandong University), P. R. China. His research interests include theory and applications of D-PMU, and power system stability and control.

Hengxu Zhang (M'06) received his B.E. degree in electrical engineering from Shandong University of Technology, in 1998, and his M.S. and Ph.D. in electrical engineering from Shandong University, in 2000 and 2003, respectively. He is now a professor with the Key Laboratory of Power System Intelligent Dispatch and Control of the Ministry of Education (Shandong University), P. R. China. His main research interests are power system security and stability assessment, power system monitoring and numerical simulation.

Qiuwei Wu (M'08–SM'15) received the Ph.D. degree in power system engineering from Nanyang Technological University, Singapore, in 2009. He is an Associate Professor with the Department of Electrical Engineering, Technical University of Denmark. He is also a Visiting Professor named by Y. Xue, with Shandong University, China. His research interests are integration of wind power and electric vehicle into power systems, active distribution networks, and real time power system simulation and analysis.

Vladimir Terzija (M'95, SM'2000, F'16) was born in Donji Baraci (former Yugoslavia). He received the Dipl-Ing., M.Sc., and Ph.D. degrees in electrical engineering from the University of Belgrade, Belgrade, Serbia, in 1988, 1993, and 1997, respectively. He is the Engineering and Physical Science Research Council Chair Professor in Power System Engineering with the School of Electrical and Electronic Engineering, The University of Manchester, Manchester, U.K., where he has been since 2006. From 1997 to 1999, he was an Assistant Professor at the University of Belgrade, Belgrade, Serbia. From 2000 to 2006, he was a Senior Specialist for switchgear and distribution automation with ABB AG, Inc., Ratingen, Germany. His current research interests include smart grid application of intelligent methods to power system monitoring, control, and protection; wide-area monitoring, protection, and control; switchgear and fast transient processes; and digital signal processing applications in power systems. Prof. Terzija is the Editor-in-Chief of the International Journal of Electrical Power and Energy Systems, an Alexander von Humboldt Fellow, as well as a DAAD and Taishan Scholar.

Wei Xie received the B.Sc. degree in Shanghai Jiaotong University in 1990. He is currently the chief engineer of the State Grid Shanghai Municipal Electric Power Company, his current research interests include renewable energy integration of smart grid and power storage technology, management of the power supply company.

Chen Fang received the B.Sc. and Ph.D. degrees from the Department of Electrical Engineering, Tsinghua University, Beijing, China, in 2006 and 2011, respectively.
He is currently an Electrical Engineer with the Electric Power Research Institute, State Grid Shanghai Municipal Electric Power Company, Shanghai, China. His current research interests include renewable energy integration of smart grid and power storage technology.